Electron-spin polarization in symmetric type-II quantum wells from bulk inversion asymmetry

A. E. Botha* and M. R. Singh†
Department of Physics and Astronomy, University of Western Ontario, London, Ontario, Canada N6A 3K7
(Received 2 May 2002; revised manuscript received 19 November 2002; published 30 May 2003)

The effect of the bulk inversion asymmetry on electron-spin polarization by resonant tunneling in symmetric, nonmagnetic, type-II semiconductor quantum wells is investigated within the envelope function approximation. A 14×14 $\mathbf{k}\cdot\mathbf{p}$ matrix Hamiltonian is used which includes the nonparabolicity and spin-split nature of the energy-band structure. Spin-dependent boundary conditions are derived and the transfer-matrix method is applied to obtain analytical expressions for the electron-spin polarization in single- and double-quantum wells. Numerical calculations of the polarization are performed for quantum well systems made from InAs and GaSb. It is shown that the inversion asymmetry of the bulk materials can produce electron-spin polarizations of up to 90% for oblique tunneling.

DOI: 10.1103/PhysRevB.67.195334 PACS number(s): 72.25.Mk, 72.20.Jv, 73.23.Hk, 73.40.Gk

I. INTRODUCTION

The electron transport properties of low-dimensional nanostructures have attracted a great deal of experimental and theoretical interest,[1–8] and considerable effort has been spent studying the electron-spin polarization in a wide variety of structures.[9–16] Spin-dependent tunneling coefficients and tunneling currents are potentially useful for improving existing spin-dependent optoelectronic devices or for predicting entirely new spintronic transport devices.

Other than electron-spin polarization by the application of a constant magnetic field, zero-field spin-dependent intraband tunneling can occur because of the spin-orbit interaction.[17,18] Such zero-field splitting has two distinct contributions: (1) microscopic, originating from the lack of inversion symmetry in the bulk material, and (2) macroscopic, originating from asymmetry in the confining potential of the nanostructure. The second contribution is often referred to as the Rashba splitting, an effect which is negligible in symmetric quantum wells.[19–21] Most work on electron-spin polarization has focused on the effects of applying a magnetic field to type-I or type-II semiconductor nanostructures, and the contributing physical processes are by now relatively well understood. By contrast, few researchers appear to have studied the zero-field splitting with the view of elucidating the microscopic mechanism of electron-spin-polarized transport across nonmagnetic type-II semiconductor quantum wells.[22,23]

In order to take into account the bulk inversion asymmetry, as in this paper, it is essential to use, at least, a 14×14 $\mathbf{k}\cdot\mathbf{p}$ matrix Hamiltonian (as opposed to the more familiar 8×8 Kane model).[24,25] The Kane model on its own does not account for inversion asymmetry in the bulk materials.[26,27] Although the Kane model may be used to calculate the Rashba contribution to electron-spin polarization, the effect of the microscopic k^3 contribution has in the past been neglected or estimated using perturbation theory.[28,29] While such approximations may be acceptable in type-I quantum wells, where the tunneling occurs between conduction bands, they are less accurate for type-II quantum wells where the tunneling occurs between the conduction band of one material and the valence band of the other material. Rather than including the effects of higher bands via perturbation theory, the 14-band model accounts for these bands explicitly. It can thus describe the band structure further away from $\mathbf{k}=0$ more accurately.

In this paper, the resonant tunneling and resulting electron-spin polarization in symmetric, nonmagnetic, type-II, semiconductor quantum wells are investigated by using a 14-band matrix Hamiltonian. This model Hamiltonian includes the nonparabolicity and nonsphericity of the energy-band structure, and accounts for the spin splitting from the inversion asymmetry of the bulk materials. It also takes into account anisotropy in the splitting with respect to different directions of $\mathbf{k}_\parallel$, the component of the wave vector that lies in the plane of the heterointerface (perpendicular to the growth direction). The 14×14 Hamiltonian is algebraically reduced to a 2×2 pseudomatrix Hamiltonian that involves only two of the original 14 envelope functions—a result which we believe is different. Numerical results are presented for quantum wells made from InAs and GaSb. It is found that the zero-field spin splitting due to the bulk inversion asymmetry is comparable to the spin splitting that can be produced by the application of a uniform magnetic field of about 3 T.[30,31] In the absence of a magnetic field, it is found that electron-spin polarizations of up to 90% can occur for oblique tunneling, i.e., when the in-plane wave vector $\mathbf{k}_\parallel=(k_x,k_y)\neq\mathbf{0}$. Because of a shortage in experimental data for symmetric quantum wells made from InAs and GaSb, a detailed experimental comparison with our theoretical predictions is difficult at present. Future fabrication of symmetric quantum wells, into which electrons can be injected at arbitrary angles with respect to the growth direction, may permit a direct comparison with the theoretical results presented here.

II. THEORETICAL FORMULATION

The 14×14 $\mathbf{k}\cdot\mathbf{p}$ Schrödinger equation for a zinc-blende semiconductor material can be written as[32]

$$\begin{pmatrix} H_1^+ & H_2^+ \\ H_2^- & H_1^- \end{pmatrix}\mathbf{\Phi}=0, \tag{1}$$

where $\mathbf{\Phi}$ is a column matrix of envelope functions denoted by $\phi_1,\phi_2,\ldots,\phi_{14}$. The 14×14 matrix Hamiltonian to the left of $\mathbf{\Phi}$ is given in natural units[33] by

$$H_1^{\pm}=\begin{pmatrix} A & 0 & 0 & \frac{P_1 k_{\mp}}{\sqrt{3}} & 0 & \frac{Q k_z}{\sqrt{3}} & 0 \\ 0 & A & 0 & \mp P_1 k_{\pm} & \frac{-Q k_z}{\sqrt{3}} & 0 & \frac{-Q k_z}{\sqrt{3/2}} \\ 0 & 0 & B & \frac{P_1 k_{\mp}}{\sqrt{3/2}} & 0 & \frac{Q k_z}{\sqrt{3/2}} & 0 \\ \frac{P_1 k_{\pm}}{\sqrt{3}} & \mp P_1 k_{\mp} & \frac{P_1 k_{\pm}}{\sqrt{3/2}} & C & \frac{P_0 k_{\pm}}{\sqrt{3}} & \mp P_0 k_{\mp} & \frac{P_0 k_{\pm}}{\sqrt{3/2}} \\ 0 & \frac{-Q k_z}{\sqrt{3}} & 0 & \frac{P_0 k_{\mp}}{\sqrt{3}} & D & 0 & 0 \\ \frac{Q k_z}{\sqrt{3}} & 0 & \frac{Q k_z}{\sqrt{3/2}} & \mp P_0 k_{\pm} & 0 & D & 0 \\ 0 & \frac{-Q k_z}{\sqrt{3/2}} & 0 & \frac{P_0 k_{\mp}}{\sqrt{3/2}} & 0 & 0 & F \end{pmatrix}, \tag{2}$$

and

$$H_2^{\pm}=\pm\begin{pmatrix} 0 & 0 & 0 & \frac{-P_1 k_z}{\sqrt{3/2}} & 0 & \frac{-Q k_{\mp}}{\sqrt{3/2}} & \pm Q k_{\pm} \\ 0 & 0 & 0 & 0 & \frac{\mp Q k_{\mp}}{\sqrt{3/2}} & 0 & \frac{Q k_{\mp}}{\sqrt{3}} \\ 0 & 0 & 0 & \frac{P_1 k_z}{\sqrt{3}} & \mp Q k_{\pm} & \frac{Q k_{\mp}}{\sqrt{3}} & 0 \\ \frac{P_1 k_z}{\sqrt{3/2}} & 0 & \frac{-P_1 k_z}{\sqrt{3}} & 0 & \frac{P_0 k_z}{\sqrt{3/2}} & 0 & \frac{P_0 k_z}{\sqrt{3}} \\ 0 & \frac{Q k_{\mp}}{\sqrt{3/2}} & \mp Q k_{\pm} & \frac{-P_0 k_z}{\sqrt{3/2}} & 0 & 0 & 0 \\ \frac{Q k_{\mp}}{\sqrt{3/2}} & 0 & \frac{Q k_{\mp}}{\sqrt{3}} & 0 & 0 & 0 & 0 \\ \pm Q k_{\pm} & \frac{-Q k_{\mp}}{\sqrt{3}} & 0 & \frac{P_0 k_z}{\sqrt{3}} & 0 & 0 & 0 \end{pmatrix}. \tag{3}$$

In the preceding equations, $A=E_1+\Delta_1-E$, $B=E_1-E$, $C=-E$, $D=-E_0-E$, and $F=-E_0-\Delta_0-E$. The components of the wave vector, with respect to the three crystal axes **a**[100], **b**[010], and **c**[001] are denoted by k_x, k_y, and k_z, respectively, and we have used the standard notation $k_{\pm}=(k_x \pm i k_y)/\sqrt{2}$. As shown in Fig. 1, the fundamental energy gap E_0 is measured between the conduction-band minimum and the valence-band maximum, E_1 is the energy gap between the conduction-band minimum and the split-off electron band, Δ_0 is the spin-orbit coupling in the valence bands, and Δ_1 is the spin-orbit coupling in the conduction bands. The interband matrix elements P_0, P_1, and Q model the nonparabolicity and nonsphericity of the energy-band structure. E is the carrier energy measured with respect to the conduction-band minimum of the material (see Fig. 1).

Equation (1) constitutes a set of 14 coupled linear equations involving 14 envelope functions. Twelve of these equations can be used to express ϕ_1, ϕ_2, ϕ_3,

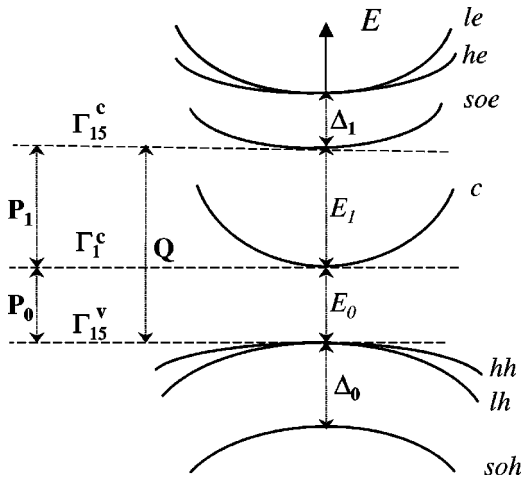

FIG. 1. Schematic energy-band structure for bulk zinc-blende semiconductors showing some of the parameters used in the 14 $\times$14 $\mathbf{k}\cdot\mathbf{p}$ matrix Hamiltonian. These bands are sometimes referred to by the labels on the right side of the figure: *le*-light electron, *he*-heavy electron, *soe*-split off electron, *c*-conduction electron, *hh*-heavy hole, *lh*-light hole, and *soh*-split off hole. In general, when $k_\parallel \neq 0$, the spin degeneracy is removed (See, for example, Fig. 2, which shows the spin splitting) by lack of inversion symmetry in the bulk material. This inversion asymmetry originates from the polarity of the bonds in the material.

$\phi_5, \ldots, \phi_{10}\phi_{12}\phi_{13}$, and ϕ_{14} as linear combinations of ϕ_4 and ϕ_{11}. Resubstitution then produces a set of two coupled linear equations involving only ϕ_4 and ϕ_{11}. This 2×2 system of equations is algebraically equivalent to the original 14×14 system and is given by

$$\begin{pmatrix} \gamma-\chi-\lambda & h \\ h^\dagger & \gamma-\chi+\lambda \end{pmatrix}\begin{pmatrix} \phi_4 \\ \phi_{11} \end{pmatrix}=0, \tag{4}$$

where

$$\gamma=3A^2BCD^2F,$$

$$\chi=g_1(k_z^2+2k_+k_-)+g_4(4k_+^2k_-^2+k_z^4)+g_2k_z^2k_-k_+ -g_6(8k_+^3k_-^3+k_z^6-2k_z^4k_+k_--4k_z^2k_+^2k_-^2),$$

$$\lambda=g_3k_z^2\sqrt{k_+k_-}+g_5(k_z^2k_+^2k_--k_z^4k_-),$$

$$h=\sqrt{2}g_3k_zk_+k_-+g_7(k_z^3k_-k_+-2k_zk_+^2k_-^2), \tag{5}$$

and

$$g_1=AD[(ABD+2ABF)P_0^2+(ADF+2BDF)P_1^2 +2C(BD+AF+BF)Q^2],$$

$$g_2=\frac{8}{3}[A(AD-BD-AF+BF)P_0^2Q^2 +D(AD-BD-AF+BF)P_1^2Q^2] +\frac{2}{3}C(4AD+2BD+2AF+BF)Q^4,$$

$$g_3=4\sqrt{2}AD[BD-AF]P_0P_1Q,$$

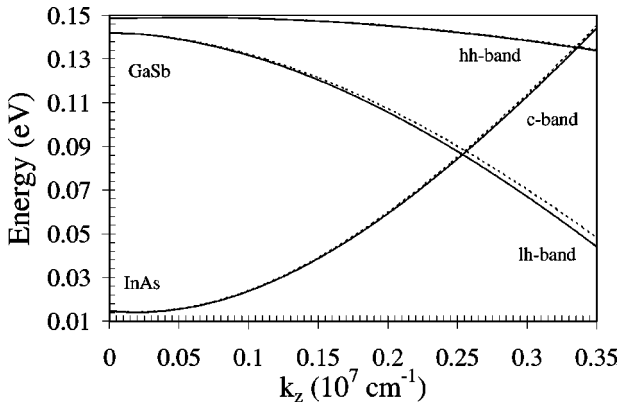

FIG. 2. Spin-split conduction and valence-bands in InAs and GaSb, respectively, as functions of k_z, for $k_\parallel=0.095\times10^7$ cm^{-1} along the [110] direction. The splitting is due to bulk inversion asymmetry. These energy bands were calculated from Eq. (7) to verify that the original eigenvalue problem posed by Eq. (1) coincides exactly with the derived result given by Eq. (7). If instead we make use of Eq. (8), in which we have neglected k^4 and higher-order terms, the calculated band structure for $0\leqslant E\leqslant0.15$ eV does not differ by more than 2% from that shown here. This is considerably more accurate than the band structure obtained from third-order perturbation theory (see also Fig. 3).

$$g_4=\frac{2}{3}[A(AD+5BD+2AF+BF)P_0^2Q^2 +D(AD++5AF+2BD+BF)P_1^2Q^2] +\frac{1}{3}C(4AD+2BD+2AF+BF)Q^4,$$

$$g_5=4\sqrt{2}[BD-AF]P_0P_1Q^3,$$

$$g_6=[(2A+B)P_0^2Q^4+(2D+F)P_1^2Q^4],$$

$$g_7=8[BD-AF]P_0P_1Q^3. \tag{6}$$

The energy eigenvalues for Eq. (4) are given by

$$\gamma=\chi\pm\sqrt{\lambda^2+h^2}, \tag{7}$$

where the positive sign is for spin-up carriers and the negative sign is for spin-down carriers.

In Fig. 2, we have used Eq. (7) to plot the spin-split conduction-band in InAs and the spin-split heavy-hole and light-hole bands in GaSb against k_z, for $k_x=k_y=0.067\times10^7\text{cm}^{-1}$ (or $k_\parallel=\sqrt{2k_+k_-}=0.095\times10^7\text{cm}^{-1}$ along the [110] direction).[34] We have also calculated these same bands by solving the energy eigenvalues numerically, directly from Eq. (1). The resulting bands are identical to those shown in Fig. 2.

If we neglect terms in Eq. (4) that are fourth order or higher in the wave vector components, the same energy bands (those shown in Fig. 2) can be calculated with an error of less than 2%. This has been verified by numerical calculations. For the purposes of the calculations that follow, we shall therefore consider only the terms in Eq. (4), which are less than or equal to third order in the wave vector components. With this approximation, Eq. (4) reduces to

$$\begin{pmatrix} \xi_1(k_z^2+2k_+k_-)+\xi_2 k_z^2\sqrt{k_+k_-}-C & -\sqrt{2}\xi_2 k_z k_+ k_- \\ -\sqrt{2}\xi_2 k_z k_- k_+ & \xi_1(k_z^2+2k_+k_-)-\xi_2 k_z^2\sqrt{k_+k_-}-C \end{pmatrix}\begin{pmatrix} \phi_4 \\ \phi_{11} \end{pmatrix}=0, \tag{8}$$

where $\xi_1=g_1C/\gamma$ and $\xi_2=g_3C/\gamma$. The eigenvalues of Eq. (8) are given by

$$\gamma=g_1(k_z^2+2k_+k_-)\pm\sqrt{g_3^2k_z^4k_+k_-+2g_3^2k_z^2k_+^2k_-^2}. \tag{9}$$

Equation (8) describes the energy-band structure of the bulk material, with the zero of carrier energy $E=0$ measured with respect to the conduction-band minimum of the material. We now consider a type-II quantum well made from InAs and GaSb. Since the conduction-band minimum of InAs lies at an energy of $V_0=0.150$ eV below the light-hole or heavy-hole valence-band maxima of the GaSb material, a so-called negative or crossedgap configuration, charge transfer occurs. This produces intrinsic carriers on either side of the hetero-interface, and gives rise to activationless generation and recombination.[15] In an *n*-type single quantum well InAs/GaSb/InAs, electrons with energy $0\leqslant E\leqslant V_0$ can tunnel through the structure. Similarly in a *p*-type quantum well GaSb/InAs/GaSb, hole resonant tunneling can occur.

We choose the zero of carrier energy $E=0$ in the quantum well to coincide with the zero of carrier energy in InAs, i.e., the conduction-band minimum of InAs. With respect to the band structure of GaSb, the zero of carrier energy in the quantum well then lies at an energy of $V_0+E_0^{\mathrm{B}}$ below the conduction-band minimum of GaSb. Thus, the carrier energy in GaSb is written as $E-V_0-E_0^{\mathrm{B}}$. Note that here we have added a superscript B to denote that E_0^{B} is the fundamental energy gap of GaSb (referred to as material B). Note that the parameters such as $E_0E_1\ldots,P_0P_1$, and Q, are different for each material (see the first paragraph of Sec. III).

We apply Eq. (8) to a single-quantum well InAs/GaSb/InAs grown in the z direction. For notational purposes we will denote the layers in this well by $A/B/C$, where C and A both stand for InAs and B stands for GaSb. The envelope functions $\phi_4^{\mathrm{A}}(z),\phi_{11}^{\mathrm{A}}(z)$ and $\phi_4^{\mathrm{B}}(z),\phi_{11}^{\mathrm{B}}(z)$ have to be joined smoothly across the interface A/B. Assume that this interface lies in the x-y plane $(z=0)$, while the second interface, B/C, lies parallel to the first at $z=d_B$. With this choice, the solution of Eq. (8) inside layer $(j=A,B,C)$ can be written in terms of a linear combination of an incident and reflected plane wave with coefficients $I_j^{\pm}$ and $R_j^{\pm}$, respectively.

$$\begin{pmatrix} \phi_4^j(z) \\ \phi_{11}^j(z) \end{pmatrix}^{\pm}=\begin{pmatrix} \alpha_j^{\pm} \\ \beta_j^{\pm} \end{pmatrix}[I_j^{\pm}\exp(ik_z^{j\pm}z)+R_j^{\pm}\exp(-ik_z^{j\pm}z)], \tag{10}$$

where $k_z^{j\pm}$ is calculated using Eq. (9). The spin components[35] $\alpha_j^{\pm}$ and $\beta_j^{\pm}$ are given by

$$\frac{\alpha_j^{\pm}}{\beta_j^{\pm}}=\mp\left(\tan\frac{\eta_j}{2}\right)^{\mp 1}, \tag{11}$$

where $\tan\eta_j=h_j/\lambda_j$.

We can obtain relationships between the coefficients in the three different layers by applying suitable boundary conditions[36,37] at the interfaces $z=0$ and $z=d_{\mathrm{B}}$. Difficulties associated with deriving appropriate boundary conditions for the envelope wave functions have recently been reviewed.[38–40] We make use of well-established boundary conditions that satisfy two fundamental physical requirements: (1) continuity of the envelope wavefunctions at the interface and (2) continuity of the probability currents at the interface.[41] At $z=0$, the first of these two requirements can be expressed mathematically as

$$\begin{pmatrix} \phi_4^{\mathrm{A}}(z) \\ \phi_{11}^{\mathrm{A}}(z) \end{pmatrix}^{\pm}_{z=0}=\begin{pmatrix} \phi_4^{\mathrm{B}}(z) \\ \phi_{11}^{\mathrm{B}}(z) \end{pmatrix}^{\pm}_{z=0}. \tag{12}$$

To express the second requirement mathematically, we follow the method outlined in Refs. 30,31,41,42. The result for the $z=0$ interface is given by

$$\begin{pmatrix} (\xi_1^{\mathrm{A}}+2\xi_2^{\mathrm{A}}k_+)\nabla_z & -i\xi_2^{\mathrm{A}}k_+k_- \\ -i\xi_2^{\mathrm{A}}k_+k_- & (\xi_1^{\mathrm{A}}-2\xi_2^{\mathrm{A}}k_+)\nabla_z \end{pmatrix}\begin{pmatrix} \phi_4^{\mathrm{A}}(z) \\ \phi_{11}^{\mathrm{A}}(z) \end{pmatrix}^{\pm}_{z=0}$$
$$=\begin{pmatrix} (\xi_1^{\mathrm{B}}+2\xi_2^{\mathrm{B}}k_+)\nabla_z & -i\xi_2^{\mathrm{B}}k_+k_- \\ -i\xi_2^{\mathrm{B}}k_+k_- & (\xi_1^{\mathrm{B}}-2\xi_2^{\mathrm{B}}k_+)\nabla_z \end{pmatrix}\begin{pmatrix} \phi_4^{\mathrm{B}}(z) \\ \phi_{11}^{\mathrm{B}}(z) \end{pmatrix}^{\pm}_{z=0}, \tag{13}$$

where the quantities ξ_1^{A}, ξ_2^{A}, ξ_1^{B}, and ξ_2^{B} are obtained from their definitions by using the appropriate parameter values for each material (see the first paragraph of Sec. III). Similar boundary conditions apply to the interface B/C located at $z=d_{\mathrm{B}}$. Notice that if $\mathbf{k}_{\parallel}=\mathbf{0}$, then the boundary conditions reduce to the well-known BenDaniel-Duke boundary conditions,[43] with effective masses $(2\xi_1^{\mathrm{A}})^{-1}$ and $(2\xi_1^{\mathrm{B}})^{-1}$. We can now apply the transfer-matrix method to the boundary conditions to obtain the mathematical relationships between the plane-wave coefficients for each layer of the single-quantum well $A/B/C$. The coefficients $I_{\mathrm{A}}^{\pm}$ and $R_{\mathrm{A}}^{\pm}$ of the left-hand InAs layer (denoted by A) can be expressed in terms of the coefficients $I_{\mathrm{C}}^{\pm}$ and $R_{\mathrm{C}}^{\pm}$ of the right-hand InAs layer (denoted by C). The result of this calculation is

$$\begin{pmatrix} I_{\mathrm{A}}^{\pm} \\ R_{\mathrm{A}}^{\pm} \end{pmatrix}=M_{\mathrm{SQW}}^{\pm}\begin{pmatrix} I_{\mathrm{C}}^{\pm} \\ R_{\mathrm{C}}^{\pm} \end{pmatrix}, \tag{14}$$

where (after setting $A=C$) the 2×2 matrix, $M_{\mathrm{SQW}}^{\pm}=M_{\mathrm{AB}}^{\pm}M_{\mathrm{BB}}^{\pm}M_{\mathrm{BA}}^{\pm}$, and the transfer matrices are given by

$$M_{\mathrm{AB}}^{\pm}=\frac{1}{\kappa_1^{\mathrm{A}\pm}+\kappa_2^{\mathrm{A}\pm}}\begin{pmatrix} \kappa^{\pm}\kappa_2^{\mathrm{A}\pm}+\kappa_3^{\mathrm{B}\pm}\kappa^{\pm}\kappa_2^{\mathrm{A}\pm}-\kappa_4^{\mathrm{B}\pm} & \\ \kappa^{\pm}\kappa_1^{\mathrm{A}\pm}-\kappa_3^{\mathrm{B}\pm}\kappa^{\pm}\kappa_1^{\mathrm{A}\pm}+\kappa_4^{\mathrm{B}\pm} & \end{pmatrix}, \tag{15}$$

$$M_{\mathrm{BB}}^{\pm}=\begin{pmatrix}\exp(-ik_z^{\mathrm{B}\pm}d_{\mathrm{B}}) & 0\\ 0 & \exp(+ik_z^{\mathrm{B}\pm}d_{\mathrm{B}})\end{pmatrix}, \tag{16}$$

and

$$M_{\mathrm{BA}}^{\pm}=\frac{1}{\kappa_1^{\mathrm{B}\pm}+\kappa_2^{\mathrm{B}\pm}}\begin{pmatrix}\kappa^{\pm}\kappa_2^{\mathrm{B}\pm}+\kappa_3^{\mathrm{A}\pm}\kappa^{\pm}\kappa_2^{\mathrm{B}\pm}-\kappa_4^{\mathrm{A}\pm}\\ \kappa^{\pm}\kappa_1^{\mathrm{B}\pm}-\kappa_3^{\mathrm{A}\pm}\kappa^{\pm}\kappa_1^{\mathrm{B}\pm}+\kappa_4^{\mathrm{A}\pm}\end{pmatrix}. \tag{17}$$

Here

$$\kappa^{\pm}=\alpha_{\mathrm{A}}^{\pm}\alpha_{\mathrm{B}}^{\pm}+\beta_{\mathrm{A}}^{\pm}\beta_{\mathrm{B}}^{\pm},$$

$$\kappa_1^{\mathrm{A}\pm}=\xi_1^{\mathrm{A}}k_z^{\mathrm{A}\pm}+2\xi_2^{\mathrm{A}}k_{\pm}k_z^{\mathrm{A}\pm}(\alpha_{\mathrm{A}}^{\pm}\alpha_{\mathrm{A}}^{\pm}-\beta_{\mathrm{A}}^{\pm}\beta_{\mathrm{A}}^{\pm})-2\xi_2^{\mathrm{A}}k_{\pm}\alpha_{\mathrm{A}}^{\pm}\beta_{\mathrm{A}}^{\pm},$$

$$\kappa_2^{\mathrm{A}\pm}=\xi_1^{\mathrm{A}}k_z^{\mathrm{A}\pm}+2\xi_2^{\mathrm{A}}k_{\pm}k_z^{\mathrm{A}\pm}(\alpha_{\mathrm{A}}^{\pm}\alpha_{\mathrm{A}}^{\pm}-\beta_{\mathrm{A}}^{\pm}\beta_{\mathrm{A}}^{\pm})+2\xi_2^{\mathrm{A}}k_{\pm}\alpha_{\mathrm{A}}^{\pm}\beta_{\mathrm{A}}^{\pm},$$

$$\begin{aligned}\kappa_3^{\mathrm{B}\pm}&=\kappa\xi_1^{\mathrm{B}}k_z^{\mathrm{B}\pm}+2\xi_2^{\mathrm{B}}k_z^{\mathrm{B}\pm}k_{\pm}(\alpha_{\mathrm{A}}^{\pm}\alpha_{\mathrm{B}}^{\pm}-\beta_{\mathrm{A}}^{\pm}\beta_{\mathrm{B}}^{\pm})\\&\quad-\xi_2^{\mathrm{A}}k_{\pm}(\alpha_{\mathrm{A}}^{\pm}\beta_{\mathrm{B}}^{\pm}+\alpha_{\mathrm{B}}^{\pm}\beta_{\mathrm{A}}^{\pm}),\\ \kappa_4^{\mathrm{B}\pm}&=\kappa\xi_1^{\mathrm{B}}k_z^{\mathrm{B}\pm}+2\xi_2^{\mathrm{B}}k_z^{\mathrm{B}\pm}k_{\pm}(\alpha_{\mathrm{A}}^{\pm}\alpha_{\mathrm{B}}^{\pm}-\beta_{\mathrm{A}}^{\pm}\beta_{\mathrm{B}}^{\pm})\\&\quad+\xi_2^{\mathrm{B}}k_{\pm}(\alpha_{\mathrm{A}}^{\pm}\beta_{\mathrm{B}}^{\pm}+\alpha_{\mathrm{B}}^{\pm}\beta_{\mathrm{A}}^{\pm}).\end{aligned} \tag{18}$$

The expressions for $\kappa_1^{\mathrm{B}\pm}$, $\kappa_2^{\mathrm{B}\pm}$, $\kappa_3^{\mathrm{A}\pm}$, $\kappa_4^{\mathrm{A}\pm}$ are obtained by interchanging *A* and *B*in Eqs. (18). We can now define the spin-dependent transmission probability, $T^{\pm}(E,\mathbf{k}_{\parallel})$, as

$$T^{\pm}(E,\mathbf{k}_{\parallel})=\frac{(I_{\mathrm{A}_3}^{\pm})(I_{\mathrm{A}_3}^{\pm})^*}{(I_{\mathrm{A}_1}^{\pm})(I_{\mathrm{A}_1}^{\pm})^*}=|(M_{\mathrm{SQW}}^{\pm})_{11}|^{-2}. \tag{19}$$

Notice that the transmission probability depends on the direction and magnitude of the in-plane wave vector. The spin-dependent transmission probability for a double-quantum well is obtained by replacing $(M_{\mathrm{SQW}}^{\pm})_{11}$, in Eq. (18), by $(M_{\mathrm{DQW}}^{\pm})_{11}$, where $M_{\mathrm{DQW}}^{\pm}=M_{\mathrm{SQW}}^{\pm}M_{\mathrm{BB}}^{\pm}M_{\mathrm{SQW}}^{\pm}$.

In experiments, a beam of unpolarized electrons may be injected into a quantum well. Depending on the carrier energy E and on the magnitude and direction of $\mathbf{k}_{\parallel}\neq\mathbf{0}$, an unpolarized electron beam could be polarized by resonant tunneling because of the spin splitting in the resonant energy states. It is therefore of interest to define the electron-spin polarization[23] as

$$P(E,\mathbf{k}_{\parallel})=\frac{T^{+}(E,\mathbf{k}_{\parallel})-T^{-}(E,\mathbf{k}_{\parallel})}{T^{+}(E,\mathbf{k}_{\parallel})+T^{-}(E,\mathbf{k}_{\parallel})}. \tag{20}$$

This polarization provides a comparison between the tunneling probabilities for spin-up and spin-down carriers. In nonmagnetic quantum wells with perfect inversion symmetry in the band-gap engineering, the polarization is due to the inversion asymmetry of the bulk materials. The inversion asymmetry in the bulk materials is a result of bond polarity.[22]

III. RESULTS AND DISCUSSION

In numerical calculations, we make use of parameter values obtained from Refs. 44,45. In units of eV, the parameter values for InAs are $V_0=0.150$, $E_0^{\mathrm{A}}=0.4127$, $E_1^{\mathrm{A}}=4.390$, $\Delta_0^{\mathrm{A}}=0.380$, $\Delta_1^{\mathrm{A}}=0.240$, $P_0^{\mathrm{A}}=21.60$, $P_1^{\mathrm{A}}=5.20$, and $Q^{\mathrm{A}}=15.82$. The parameter values for GaSb are $V_0=0.150$, $E_0^{\mathrm{B}}=0.8143$, $E_1^{\mathrm{B}}=3.191$, $\Delta_0^{\mathrm{B}}=0.758$, $\Delta_1^{\mathrm{B}}=0.210$, $P_0^{\mathrm{B}}=27.50$, $P_1^{\mathrm{B}}=11.50$, and $Q^{\mathrm{B}}=15.11$.

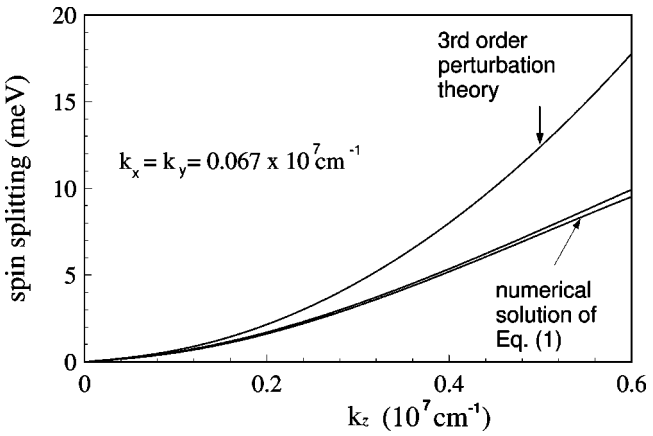

FIG. 3. The spin splitting in the valence-band of bulk GaSb as a function of k_z with $k_x=k_y=0.067\times10^7$ cm^{-1}. We have used the same parameters (listed at the beginning of Sec. III) to calculate the three curves shown in Fig. 3. Each curve is, however, calculated by a different method: by third-order perturbation theory (top curve), by numerical solution of the eigenvalues of Eq. (1) (bottom curve), and by numerical solution of Eq. (9) (middle curve).

The present formulation is more accurate than the third-order perturbation techniques. The spin-split band structure, as calculated from third-order perturbation theory, for example,[18,27,29,46] differs by more than 10% from that shown in Fig. 2. As indicated in Sec. II, the same spin-split band structure can be calculated according to our present method, based on the approximation used to obtain Eq. (8), and the resulting band structure differs by less than 2% over the same carrier energy range ($0\leqslant E\leqslant0.150$ eV) shown in Fig. 2. The spin splitting that we calculate from Eq. (8) is found to be more accurate than that which is predicted by third-order perturbation theory. This is illustrated in Fig. 3 where the spin splitting in the valence-band of bulk GaSb is shown as a function of k_z, with $k_x=k_y=0.067\times10^7$ cm^{-1}. We have used the same parameters for each of the three curves shown in Fig. 3. The top curve was calculated from the well-known formula[26] $\Delta E=2\gamma_c[k^2(k_x^2k_z^2+k_y^2k_x^2+k_z^2k_y^2)-9k_x^2k_y^2k_z^2]^{1/2}$. This formula can be derived from the 14-band model using third-order perturbation theory with respect to k terms.[27,46] The middle curve in Fig. 3 was calculated by solving the eigenvalues of Eq. (1) numerically, and the bottom curve was calculated numerically from Eq. (9). The discrepancy between the spin splitting predicted by third-order perturbation theory and the exact numerical solution to Eq. (1) is significantly more than that predicted by Eq. (9). Note that Eq. (9) takes into account the band nonparabolicity. This can be seen though the complicated energy dependence of γ, g_1, and g_3 that appear in Eq. (9). By contrast, the famous splitting parameter γ_c does not depend on E [see also Eq. (5.7) of Ref. 8].

Figure 4 shows the bulk spin splitting as a function of $\mathbf{k}_{\parallel}[110]$ for the ground (bottom curve) and first excited (top

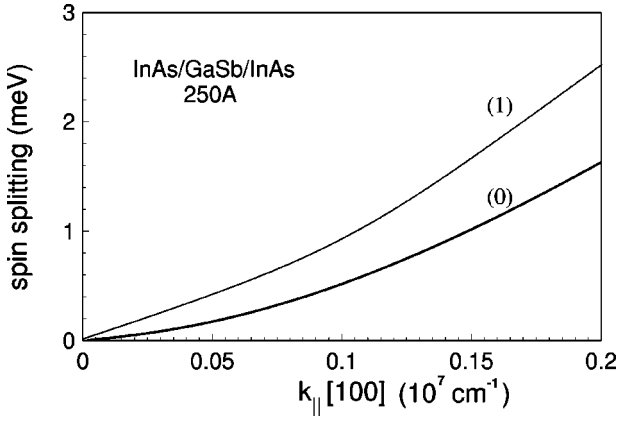

FIG. 4. The spin splitting of the ground state (0) and the first excited state (1) as a function of $k_{\|}[100]$ for a 250-Å wide quantum well InAs/GaSb/InAs.

curve) state in a 250-Å wide single-quantum well InAs/GaSb/InAs. The spin splitting of the ground state (0) is less than that of the first excited state (1). The spin splitting is calculated from the energy difference between the maxima in the corresponding transmission probability peaks, one for the spin-up (+) case, and the other for the spin-down (−), i.e., we have plotted $E^{+}(T^{+}_{\max})-E^{-}(T^{-}_{\max})$ against $\mathbf{k}_{\|}[110]$ for each resonant state.

Figure 5 illustrates how the spin splitting from bulk inversion asymmetry changes with well width. We plot the spin splitting for a single-quantum well InAs/GaSb/InAs as a function of well width, for two different values of $k_{\|}$. The top two curves in the figure are for the ground (0) and first excited (1) sub-bands when $k_{\|}=0.189\times10^{7}$ cm^{-1} in the [010] direction. The bottom curves are for the ground (0) and first excited (1) sub-bands when $k_{\|}=0.095\times10^{7}$ cm^{-1} in the [010] direction. For $d_{\mathrm{B}}<200$ Å, there is only one resonant

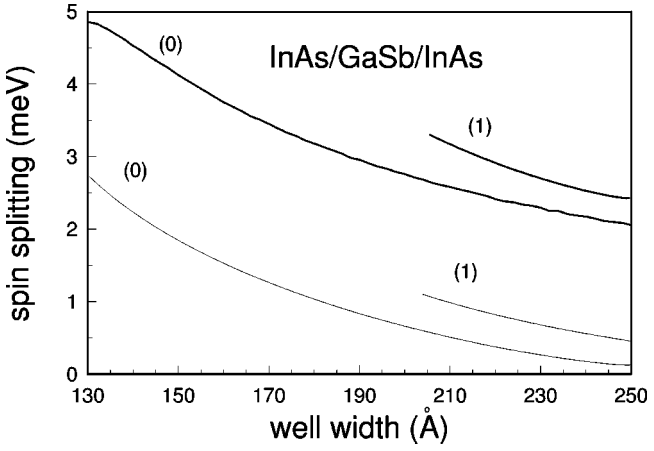

FIG. 5. Spin splitting in a quantum well InAs/GaSb/InAs from bulk inversion asymmetry as a function of the well width. The top two curves show the ground (0) and first excited (1) resonant states for $k_{\|}=0.189\times10^{7}$ cm^{-1} in the [010] direction. The bottom two curves show the ground (0) and first excited (1) resonant states for $k_{\|}=0.095\times10^{7}$ cm^{-1} in the [010] direction. The spin splitting increases as the magnitude of $\mathbf{k}_{\|}$ increases.

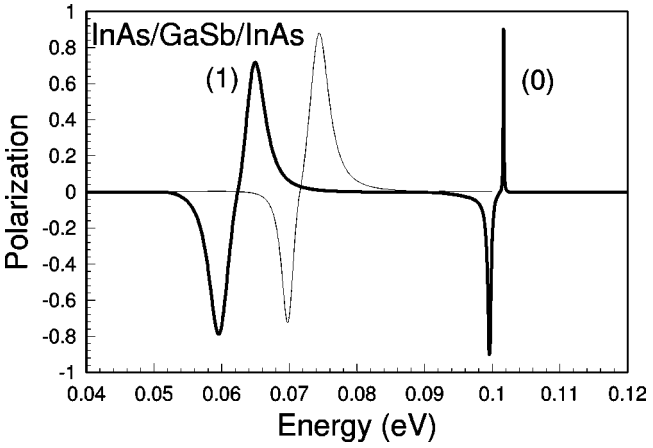

FIG. 6. Electron-spin polarization in single-quantum wells InAs/GaSb/InAs as a function of electron energy. The thin curve is for a 150-Å wide well in which the polarization arises from splitting in the ground resonant state. The thick curve is for a 250 Å well in which there is a spin-split ground (0) and first excited (1) resonant state. For both widths, $k_{\|}=0.189\times10^{7}$ cm^{-1} in the [110] direction.

state. As the well width increases beyond 200 Å another resonant state appears. It is interesting to note that the splitting shown in Figs. 4 and 5 is comparable with the extrapolated values from the experimental results reported for similar quantum wells in which the confinement potential is asymmetric, due to the epitaxial growth process.[47,48] In these experiments, the total zero-field spin splitting could be modeled purely in terms of the Rashba splitting, by neglecting the effect of bulk inversion asymmetry. According to our present model, however, the zero-field splitting due to bulk inversion asymmetry alone is not negligible in comparison to the total spin splitting. The bulk inversion asymmetry does appear to be an important contribution to the total zero-field spin splitting, irrespective of whether the band-gap engineering is symmetric or asymmetric. It is reasonable to assume that the bulk spin splitting should be roughly the same, independently of whether the confining potential is symmetric or asymmetric.[18,27,29,46] Experiments that probe only the total splitting cannot distinguish the contributions from each source.[49]

In Fig. 6, we have plotted the polarization for an InAs/GaSb/InAs quantum well. We have plotted the polarization as a function of electron energy for $k_{\|}=0.189\times10^{7}$ cm^{-1} in the [110] direction. The two curves are for well widths of $d_{\mathrm{B}}=150$ Å (thin curve) and $d_{\mathrm{B}}=250$ Å (thick curve). In the 150 Å case, the maximum and minimum in the polarization is a result of the bulk spin splitting in the ground resonant state of the well. The polarization from this state is approximately 80%. In the case of the 250 Å well, the polarization corresponding to the first excited resonance (1) is smaller than that from the ground state (0). This is a general feature of the polarization. In general, the spin splitting for the higher-order resonance states is larger than for lower-lying states (see Figs. 4 and 5, for example). Transmission peaks corresponding to higher-order resonance states are (in general) also broader than those of lower-order states. This results in smaller polarizations for the higher-order resonances.

The polarization is thus influenced by the magnitude of the spin splitting and the width of the transmission peaks. These two factors depend in turn on $\mathbf{k}_{\|}$ and also on the relative importance of the spin dependent boundary conditions. The higher-order resonances are less sensitive to the spin-dependence of the boundary conditions.[22,23]

It is interesting to note that the polarization maxima and minima for a given resonance state may not be equal in magnitude. If the resonant state lies close to the forbidden energy gap, the transmission peaks for spin up and spin down are skewed. This feature can be exploited to polarize an initially unpolarized beam of electrons.[50] For example, our calculations show that a 100-Å wide GaSb/InAs/GaSb quantum well contains no resonant bound states for spin-up electrons, but it does contain a resonant bound state for spin-down electrons. An initially unpolarized electron beam containing electrons with energy less than $\approx V_0 + E_0^{\mathrm{B}} = 0.96$ eV can thus be filtered (in energy as well as in spin) to produce a highly polarized low-energy electron beam. This phenomenon is currently of great interest because of its many potential applications to spintronic filtering and switching devices.

In summary, we have studied the electron-spin polarization in symmetric quantum wells due to the inversion asymmetry of the bulk materials. We have reduced the 14×14 model Hamiltonian to a 2×2 pseudomatrix Hamiltonian which we then use to study tunneling without the use of perturbation theory. We neglect terms in the 2×2 system that are higher than k^3, and obtain a description of the bulk band structure which is still more accurate than most of the third-order perturbation techniques. Our calculations show that the zero-field electron-spin polarization can, in principle, be used to produce an adjustable beam of highly polarized low-energy electrons. This could have practical applications for spintronic filtering or switching devices. We have also shown that the calculated bulk spin splitting is comparable with the total zero-field spin splitting that is found experimentally for asymmetric quantum wells made from InAs and GaSb.

*Electronic address: aebotha@uwo.ca
†Electronic address: msingh@uwo.ca

[1] L. Esaki and R. Tsu, IBM J. Res. Dev. **14**, 61 (1970).
[2] R. Tsu and L. Esaki, Appl. Phys. Lett. **22**, 562 (1973).
[3] L.L. Chang, L. Esaki, and R. Tsu, Appl. Phys. Lett. **24**, 593 (1974).
[4] L.L. Chang *et al.*, Appl. Phys. Lett. **35**, 939 (1979).
[5] G.E. Marques and L.J. Sham, Surf. Sci. **113**, 131 (1982).
[6] S. Washburn, R.A. Webb, E.E. Mendez, L.L. Chang, and L. Esaki, Phys. Rev. B **31**, 1198 (1985).
[7] M.I. D'yakonov and V.Y. Kachorovskii, Sov. Phys. Semicond. **20**, 110 (1986).
[8] M. Cardona, N.E. Christensen, and G. Fasol, Phys. Rev. B **38**, 1806 (1988).
[9] Y. Rajakarunanayake, B.H. Cole, J.O. McCaldin, D.H. Chow, J.R. Soderstrom, T.C. McGill, and C.M. Jones, Appl. Phys. Lett. **55**, 1217 (1989).
[10] H. Ohno, L. Esaki, and E.E. Mendez, Appl. Phys. Lett. **60**, 3153 (1992).
[11] Y.V. Dubrovskii, Y.N. Khanin, I.A. Larkin, S.V. Morozov, T.G. Andersson, and J.R. Soderstrom, Phys. Rev. B **50**, 4897 (1994).
[12] A. Zakharova, F.T. Vasko, and V. Ryzhii, J. Phys.: Condens. Matter **6**, 7537 (1994).
[13] W.H. Lau and M.R. Singh, Solid State Commun. **100**, 359 (1996).
[14] W.H. Lau and M.R. Singh, Phys. Status Solidi B **193**, 269 (1996).
[15] A. Shik and M.R. Singh, Phys. Status Solidi A **168**, 195 (1998).
[16] A. Zakharova, S.T. Yen, and K.A. Chao, Phys. Rev. B **64**, 235332 (2001).
[17] E.A. de Andrada e Silva, G.C. La Rocca, and F. Bassani, Phys. Rev. B **50**, 8523 (1994).
[18] W. Zawadzki, P. Pfeffer, and M. Kubisa, Mol. Phys. Rep. **23**, 113 (1999).
[19] Y.A. Bychkov and E.I. Rashba, J. Phys. C **17**, 6039 (1984).
[20] E.A. de Andrada e Silva, Phys. Rev. B **46**, 1921 (1992).
[21] B. Jusserand, D. Richards, G. Allan, C. Priester, and B. Etienne, Phys. Rev. B **51**, 4707 (1995).
[22] E.A. de Andrada e Silva, G.C. La Rocca, and F. Bassani, Phys. Rev. B **55**, 16 293 (1997).
[23] E.A. de Andrada e Silva and G.C. La Rocca, Phys. Rev. B **59**, 15 583 (1999).
[24] E.O. Kane, J. Phys. Chem. Solids **1/2**, 82 (1956).
[25] E.O. Kane, J. Phys. Chem. Solids **1**, 249 (1957).
[26] W. Zawadzki, P. Pfeffer, and H. Sigg, Solid State Commun. **53**, 777 (1985).
[27] P. Pfeffer and W. Zawadzki, Phys. Rev. B **41**, 1561 (1990).
[28] M.F.H. Schuurmans and G.W. 't Hooft, Phys. Rev. B **31**, 8041 (1985).
[29] R. Eppenga and M.F.H. Schuurmans, Phys. Rev. B **37**, 10 923 (1988).
[30] M.R. Singh and A.E. Botha, Solid State Commun. **115**, 625 (2000).
[31] M.R. Singh and A.E. Botha, Phys. Status Solidi B **222**, 569 (2000).
[32] L.-H. Peng, Ph.D. thesis, Harvard University, 1994.
[33] R. McWeeny, Nature (London) **243**, 196 (1973).
[34] To convert to natural units multiply by $5.291\,772\,49\times10^{-9}$ cm.
[35] P.R. Wallace, Phys. Status Solidi B **92**, 49 (1979).
[36] G. Bastard, *Wave Mech. Applied to Semicond. Heterostructures* (Edition de Physique, Les Ulis, 1988).
[37] S. L. Chuang, *Physics of Optoelectronic Devices* (Wiley, New York, 1995).
[38] B.A. Foreman, Phys. Rev. Lett. **82**, 1339 (1999).
[39] O. Krebs and P. Voisin, Phys. Rev. Lett. **82**, 1340 (1999).
[40] E.E. Takhtamirov and V.A. Volkov, JETP **90**, 1063 (2000).
[41] A.E. Botha and M.R. Singh, Phys. Status Solidi B **231**, 437 (2002).
[42] W.H. Lau and M.R. Singh, J. Phys. C **10**, 4257 (1998).
[43] D.J. BenDaniel and C.B. Duke, Phys. Rev. **152**, 683 (1966).
[44] W.H. Lau, J.T. Olesberg, and M.E. Flatté, Condens. Matter Phys. **2**, 1 (2000).
[45] Low-temperature values obtained from the Landolt-Börnstein tables.
[46] P. Pfeffer and W. Zawadzki, Phys. Rev. B **52**, 14 332 (1995).
[47] J. Luo, H. Munekata, F.F. Fang, and P.J. Stiles, Phys. Rev. B **38**, 10 142 (1988).

[48] J. Luo, H. Munekata, F.F. Fang, and P.J. Stiles, Surf. Sci. **229**, 73 (1990).

[49] J. Luo, H. Munekata, F.F. Fang, and P.J. Stiles, Phys. Rev. B **41**, 7685 (1990).

[50] A. E. Botha and M. R. Singh, in *Proceedings of the 26th International Conference on the Physics of Semiconductors*, Edited by C. Brown (World Scientific Publishing Co. Pte. Ltd., London, 2002).